Tuning the organelle specificity and cytotoxicity of iridium(III) photosensitisers for enhanced phototheranostic applications

Zhu, Jing-Hui; Xu, Guang-Xi; Shum, Justin; Lee, Lawrence Cho-Cheung; Lo, Kenneth Kam-Wing

Published in:
Chemical Communications

Published: 21/11/2021

Document Version:
Post-print, also known as Accepted Author Manuscript, Peer-reviewed or Author Final version

Published version (DOI):
10.1039/d1cc04982h

Publication details:
Zhu, J.-H., Xu, G.-X., Shum, J., Lee, L. C.-C., & Lo, K. K.-W. (2021). Tuning the organelle specificity and cytotoxicity of iridium(III) photosensitisers for enhanced phototheranostic applications. *Chemical Communications*, *57*(90), 12008-12011. https://doi.org/10.1039/d1cc04982h

This is the accepted version of a paper published in *Chemical Communications*. This paper has been peer-reviewed but does not include the final publisher proof-corrections or journal pagination.

Zhu, J-H., Xu, G-X., Shum, J., Lee, L. C-C., & Lo, K. K-W. (2021). Tuning the organelle specificity and cytotoxicity of iridium(III) photosensitisers for enhanced phototheranostic applications. *Chemical Communications, 57*(90), 12008-12011. https://doi.org/10.1039/d1cc04982h.

COMMUNICATION

Tuning the Organelle Specificity and Cytotoxicity of Iridium(III) Photosensitisers for Enhanced Phototheranostic Applications†

Received 00th January 20xx,
Accepted 00th January 20xx

DOI: 10.1039/x0xx00000x

Jing-Hui Zhu,[a] Guang-Xi Xu,[a] Justin Shum,[a] Lawrence Cho-Cheung Lee,[a] and Kenneth Kam-Wing Lo*[abc]

Luminescent cyclometallated iridium(III) complexes with a polyhedral oligomeric silsesquioxane (POSS) unit were designed as efficient imaging reagents and photosensitisers that displayed tuneable organelle-targeting properties, minimal dark cytotoxicity and substantial photocytotoxicity even under hypoxic conditions.

Luminescent transition metal complexes continue to attract attention as bioreagents due to their inherent theranostic characteristics and remarkable photosensitising abilities.[1] However, many metal-based photosensitisers (PSs) suffer from high dark cytotoxicity,[2] which substantially impedes their bio-applicability. Additionally, photosensitisation of most transition metal complexes is based on energy transfer from their excited states to molecular oxygen (O_2) generating singlet oxygen ($^1O_2$) (Type II process),[1] which is heavily dependent on the cellular O_2 levels and is substantially reduced in efficiency under hypoxic conditions. Indeed, the cancer-inhibiting efficacy of the $^1O_2$-involving PSs has been found to be suppressed or even ineffective under hypoxia.[3–7] On the contrary, Type I process that involves electron transfer from the excited states to biological substrates to generate ROS such as $O_2^{\cdot-}$, ·OH and H_2O_2 is effective even under hypoxia due to the lower O_2-dependence enabled by the biocatalytic oxygen recycle.[8] Thus, it is important to explore new ROS photosensitisers with minimal dark cytotoxicity and elevated photocytotoxicity under hypoxia and normoxia.

Polymeric and oligomeric units have been utilised to construct photofunctional bioconjugates to minimise their possible interaction with biomolecules.[9–11] Our group have previously developed luminescent iridium(III) complexes featuring a poly(ethylene glycol) (PEG) chain[11] and a cubic polyhedral oligomeric silsesquioxane (POSS) unit[12] that display very low dark cytotoxicity but become very cytotoxic upon irradiation. However, these PEG or POSS complexes are type II PSs. Inspired by a recent study that employed metal-organic frameworks featuring an $O_2^{\cdot-}$-generating iridium(III) 2-phenylquinoline-4-carboxylate (pqe) complex for photocatalytic sulfide oxidation,[13] we envisage that the conjugation of a cytotoxicity-attenuating POSS unit to a $O_2^{\cdot-}$-photogenerating iridium(III) pqe complex will afford new molecular materials for enhanced photocytotoxic applications.

Herein, we present the design, synthesis and characterisation of three new molecular hybrids composed of a cyclometallated iridium(III) core and a POSS unit $[Ir(pqe)_2(N^X)](PF_6)_n$ (N^X = mbpy-POSS, n = 1 (**1**); pic-POSS, n = 0 (**2**); picpy-POSS, n = 1 (**3**)) and their POSS-free counterparts (N^X = dmbpy, n = 1 (**1a**); pic, n = 0 (**2a**); picpy, n = 1 (**3a**)) (Scheme 1). Synthetic routes of the complexes are illustrated in Schemes S1–S3 (ESI†). All the complexes were purified and characterised by ^{1}H NMR, ESI-MS, IR and elemental analysis (ESI†). Upon irradiation, all the complexes exhibited intense and long-lived emission in fluid solutions at 298 K and 77 K-glass. The emission spectra are shown in Fig. S2 (ESI†), and the photophysical data are summarised in Table 1.

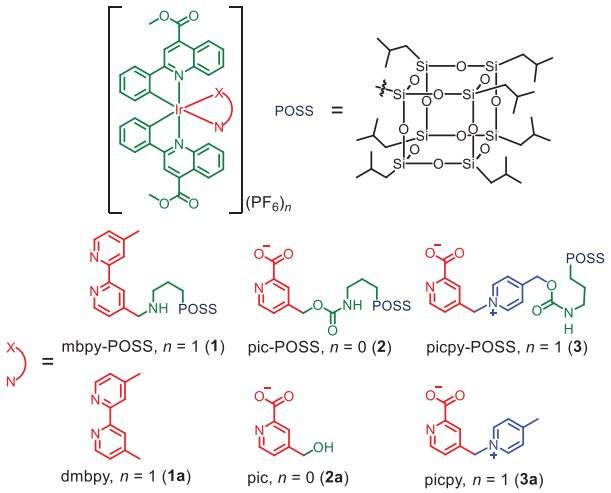

Scheme 1 Molecular structures of complexes **1**–**3** and **1a**–**3a**.

[a] Department of Chemistry, City University of Hong Kong, Tat Chee Avenue, Hong Kong, P. R. China. E-mail address: bhkenlo@cityu.edu.hk.
[b] State Key Laboratory of Terahertz and Millimetre Waves, City University of Hong Kong, Tat Chee Avenue, Hong Kong, P. R. China.
[c] Centre of Functional Photonics, City University of Hong Kong, Tat Chee Avenue, Hong Kong, P. R. China.

† Electronic Supplementary Information (ESI) available. See DOI: 10.1039/x0xx00000x

Table 1 Photophysical data of complexes **1** – **3** and **1a** – **3a** in degassed solvents at 298 K and alcohol glass at 77 K, and singlet oxygen quantum yields (Φ_Δ) of the complexes were measured in aerated CH_3CN at 298 K.

Complex	Medium (T/K)	λ_{em}/nm	τ_o[a]/μs	Φ_{em}[b]	Φ_Δ[c]	Φ_Δ[d]
1	CH_2Cl_2 (298)	623	1.36	0.07	0.44	0.42
	CH_3CN (298)	642	0.45	0.03		
	Glass[e] (77)	597, 650 sh	4.98			
1a	CH_2Cl_2 (298)	624	1.44	0.09	0.52	0.49
	CH_3CN (298)	642	0.48	0.04		
	Glass[e] (77)	597, 650 sh	5.21			
2	CH_2Cl_2 (298)	663	0.22	0.03	0.35	0.26
	CH_3CN (298)	674	0.05	0.01		
	Glass[e] (77)	621, 674 sh	5.97			
2a	CH_2Cl_2 (298)	668	0.23	0.03	0.39	0.27
	CH_3CN (298)	678	0.05	0.01		
	Glass[e] (77)	623, 674 sh	6.12			
3	CH_2Cl_2 (298)	662	0.15	0.006	0.16	0.16
	CH_3CN (298)	667	0.06	0.004		
	Glass[e] (77)	622, 674 sh	6.26			
3a	CH_2Cl_2 (298)	666	0.13	0.006	0.15	0.18
	CH_3CN (298)	674	0.06	0.004		
	Glass[e] (77)	619, 674 sh	6.34			

[a] Measured at emission maxima; [b] Reference: $[Ru(bpy)_3]Cl_2$ (Φ_{em} = 0.04 in aerated aqueous solution);[14a] [c] Reference: $[Ru(bpy)_3]Cl_2$ (Φ_Δ = 0.57 in aerated CH_3CN)[14b] and 1,3-diphenylisobenzofuran as a $^1O_2$ scavenger;[11c] [d] Determined based on $^1O_2$ fluorescence; [e] In *n*-butyronitrile glass.

The bipyridine complexes **1** and **1a** displayed orange-red emission while the picolinate complexes **2**, **2a**, **3** and **3a** exhibited deep-red emission (Table 1). The emission was ascribed to a triplet metal-to-ligand charge-transfer (^{3}MLCT) (dπ(Ir) $\rightarrow$ π^*(N^X/pqe)) excited state,[15–17] which is supported by the observed positive solvatochromism at 298 K and significant hypsochromic shifts when the samples were cooled to 77 K. The complexes showed no sign of decomposition in aerated and degassed CH_3CN upon irradiation at 450 nm (10 mW cm^{-2}) for 30 min at 298 K (Fig. S3). As expected, the emission was efficiently quenched by oxygen. However, they showed relatively moderate to low $^1O_2$ quantum yields (Φ_Δ = 0.52–0.15) (Table 1) compared to other cyclometalated iridium(III) systems,[18] and the modification with a POSS unit did not substantially affect the Φ_Δ values. Intriguingly, the complexes displayed notable photoinduced ROS generation as revealed by the fluorogenic indicator dihydrorhodamine 123 (DHR 123) (Table S2, ESI†). The bipyridine complexes **1** and **1a** exhibited the highest photoinduced ROS generation efficiencies, while the pyridinium-containing picolinate complexes **3** and **3a** showed the lowest. Also, the photoinduced ROS generation was validated by the fluorogenic photo-oxidation of DHR 123 by the excited complexes in the presence of various ROS scavengers (Table S2, ESI†). Experiments involving sodium pyruvate, D-mannitol and ebselen concluded that H_2O_2, ·OH and $ONOO^-$ did not contribute substantially to the reactive species. However, experiments using sodium azide and tiron indicated that all the complexes were efficient in the photogeneration of $O_2^{\cdot-}$,

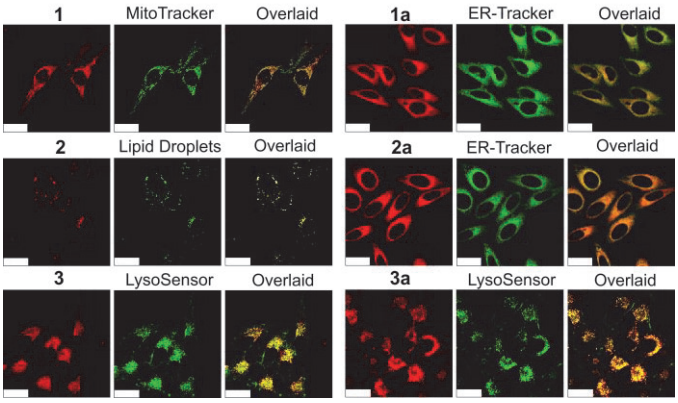

Fig. 1 LSCM images of live HepG2 cells incubated with complexes **1** – **3** (10 μM) or **1a** – **3a** (5 μM) for 3 h (for all complexes, λ_{ex} = 405 nm, λ_{em} = 600 – 750 nm) and then with organelle tracker (MitoTracker Green, 500 nM, 15 min; BODIPY 493/503, 10 μM, 15 min; LysoSensor Green, 500 nM, 15 min; or ER-Tracker Green 1 μM, 30 min. All trackers were excited at λ_{ex} = 488 nm, and collected at λ_{em} = 500 – 550 nm) at 37°C. Scale bar = 25 μm.

although complexes **1** and **1a** were also good $^1O_2$ PSs. This is in good agreement with the highest $^1O_2$ quantum yields of these two complexes (Table 1), and their least negative excited-state redox potentials ($E^\circ[Ir^{(n+1)+/n+*}]$) (*ca*. –0.70 and –0.74 V *versus* SCE for complexes **1** and **1a**, respectively, Fig. S4, ESI†).

The lipophilicity (expressed as log $P_{o/w}$ values) of the iridium(III) complexes was determined by the shake-flask method with [Ir] measured by ICP-MS (Table S4, ESI†). Due to their positive charge, the bipyridine complexes **1** and **1a** and pyridinium complexes **3** and **3a** were naturally less lipophilic than the neutral complexes **2** and **2a**. Additionally, the lipophilicity of the POSS complexes **1** – **3** was significantly increased upon modification with a POSS unit. The rather different log $P_{o/w}$ values of all these complexes were anticipated to lead to diverse intracellular distribution properties. The cellular uptake and localisation of the complexes were studied using ICP-MS and laser scanning confocal microscopy (LSCM), respectively. All the complexes readily permeated the plasma membrane and rapidly accumulated in the cytoplasm with negligible nuclear uptake (Fig. 1). Despite their structural similarity, the complexes exhibited very different organelle-targeting selectivity. The POSS complexes **1**, **2** and **3** were mainly localised in the mitochondria, lipid droplets and lysosomes, respectively (Fig. 1) with Pearson's colocalisation coefficients (PCCs) being 0.87, 0.99 and 0.77, respectively. In contrast, the POSS-free complexes **1a** and **2a** stained the endoplasmic reticulum (ER) (PCCs = 0.90 and 0.93, respectively) and complex **3a** targeted the lysosomes (PCC = 0.83) (Fig. 1). Although both complexes **3** and **3a** demonstrated lysosomal localisation, the PCC of the POSS complex **3** (0.77) was slightly smaller than that of its POSS-free counterpart **3a** (0.83), a result that may be attributed to the POSS unit in complex **3**. Summing up, the conjugation of a POSS unit to the complexes is a useful means to tune their organelle-targeting selectivity, providing an effective way to design organelle-selective bioimaging reagents and photosensitisers.

COMMUNICATION

Table 2 Cytotoxicity (IC_{50}, μM) of complexes **1** – **3** and **1a** – **3a** towards various cancer cell lines. The cells were first incubated in the dark for 24 h, incubated in the dark or upon irradiation at 450 nm (10 mW cm^{-2}) for 5 min, and subsequently incubated in the dark for 24 h

Complex	HepG2			MCF-7			U87 MG		
	Dark	Light	PI[a]	Dark	Light	PI[a]	Dark	Light	PI[a]
1	25.9 ± 1.9	2.0 ± 0.1	12.9	22.2 ± 2.7	0.8 ± 0.2	27.8	31.6 ± 1.9	2.7 ± 0.3	11.7
1a	4.8 ± 0.3	0.1 ± 0.01	48.0	2.0 ± 0.1	0.3 ± 0.04	6.7	3.1 ± 0.9	0.2 ± 0.01	15.5
2	> 100	8.3 ± 1.1	> 12.0	> 100	8.0 ± 0.9	> 12.5	> 100	16.7 ± 1.6	> 6.0
2a	8.6 ± 0.7	1.9 ± 0.2	4.5	15.3 ± 1.1	4.6 ± 0.7	3.3	10.8 ± 1.4	3.6 ± 0.3	3.0
3	25.5 ± 3.9	4.7 ± 0.2	5.4	28.8 ± 1.5	3.2 ± 1.5	9.0	35.6 ± 4.8	6.2 ± 0.23	5.7
3a	19.5 ± 2.3	2.9 ± 0.1	6.7	8.0 ± 0.1	3.4 ± 0.2	2.4	16.1 ± 2.6	3.0 ± 0.2	5.4

[a] Photocytotoxicity index (PI) = IC_{50} (dark)/IC_{50} (light).

Complexes **1** and **1a** were taken as models to evaluate the effects of the POSS unit on the uptake mechanisms. Cells pretreated with the POSS complex **1** at 4°C resulted in weaker intracellular emission than at 37°C (Fig. S5a and S5b, ESI†), suggestive of an energy-dependent pathway. Preincubation of the cells with chlorpromazine, a potent inhibitor that blockades clathrin-mediated endocytosis,[19] substantially lowered the uptake of the complex (Fig. S5c, ESI†). On the contrary, subtle alteration occurred in the uptake when the cells were pretreated with β-cyclodextrin (Fig. S5d, ESI†), an inhibitor for the caveolae-mediated endocytosis,[20] indicative of no pronounced contribution of caveolae-mediated endocytosis to the internalisation of the complex. Additionally, preincubation of a macropinocytosis inhibitor (5-(*N*-ethyl-*N*-isopropyl)amiloride)[21] led to a substantial drop in the cellular emission intensity (Fig. S5e, ESI†), demonstrative of the proactive role of macropinocytosis in the transport of the complex. Collectively, it is conceivable that the POSS complex **1** was mainly taken up via a mixed clathrin-mediated endocytotic and macropinocytotic pathway. Unexpectedly, the internalisation of complex **1a** was minimally affected by temperature and various endocytosis inhibitors (Fig. S6, ESI†), indicative of an energy-independent passive diffusion pathway.

The (photo)cytotoxicity of all the complexes towards human liver, breast and glioblast cancer cells (HepG2, MCF-7 and U87 MG) under normoxia condition was evaluated using the MTT assays. The IC_{50} values (dark) for the cationic POSS complexes **1** and **3** were similar for all three tested cell lines, while the neutral POSS complex **2** exhibited the lowest dark cytotoxicity (IC_{50} > 100 μM) (Table 2). Distinctively, the POSS-free complexes **1a** – **3a** presented much smaller IC_{50} values (dark), suggestive of higher cytotoxicity. The lower dark cytotoxicity of the POSS complexes can be ascribed to the large steric hindrance provided by the heptakis(isobutyl) POSS pendant, which refrains the complexes from interacting with biomolecules.[11,12] The lower cellular uptake of the POSS complexes should be another reason for the reduced dark cytotoxicity of the complexes (Table S5, ESI†).

Upon irradiation (450 nm, 10 mW cm^{-2}, 5 min), the IC_{50} values of all the complexes were substantially attenuated (Table 2). The anticancer efficacy of the complexes towards $CoCl_2$-induced hypoxic HepG2 cells[22] was also examined. All the complexes were slightly less cytotoxic to cells in the dark under hypoxia (Table S5, ESI†) compared with normoxia (Table 2). Lower cytotoxicity of antineoplastics towards cells under hypoxia has been attributed to hypoxia-induced drug resistance.[4,5,23,24] Although the photocytotoxicity of these complexes also decreased under hypoxia, the IC_{50} values were still in sub-μM to μM levels, attributable to photoinduced generation of ROS. This was validated by a fluorogenic ROS probe CM-H_2DCFDA. Considerable photogeneration of ROS by complexes **1** and **1a** in HepG2 cells under normoxia upon excitation at 450 nm (10 mW cm^{-2}, 5 min) was observed (Fig. S7 and S8, ESI†). Preincubation of cells with ascorbic acid (AA),[23] a scavenger for ROS, diminished the luminescence. However, negligible emission intensity changes were detected when the cells were pretreated with NaN_3, a $^1O_2$ scavenger.[23] These results testified the photogeneration of intracellular $O_2^{\cdot-}$. Similar observations were obtained when the cells were under hypoxia (Fig. S9 and S10, ESI†). Additionally, on changing from normoxia to hypoxia, the IC_{50} values (light) of complexes **2**, **2a**, **3** and **3a** increased by 1.1 to 2.1 fold only, compared with complexes **1** and **1a** (4.5 and 4.0 fold, respectively), indicating that the photocytotoxic activity of these four complexes is much less dependent on the availability of oxygen.

Since there was no simple correlation between the photocytotoxicity indexes of the complexes in different cell lines, the reduced dark cytotoxicity or elevated cytotoxicity upon irradiation may also be due to different mechanisms of action in addition to the aforementioned reasons. Thus, the cell death pathways induced by complexes **1** and **1a** were investigated as examples. The differences in plasma membrane appearance, cytoskeleton structure, and nuclear morphology of HepG2 cells pretreated with complex **1** in the dark or upon irradiation are shown in Fig. 2. Membrane

blebbing, disruptions of actin structures, and shrinkage of cell nucleus were observed, indicative of apoptotic cell death.[25,26] Other apoptotic hallmarks such as the opening of mitochondrial permeability transition pore and a decrease of mitochondrial membrane potential were also noticed (Fig. S11, ESI†).[25] The upregulation of caspase 3/7 activity[25] (Fig. S12, ESI†) further confirmed the apoptotic pathway triggered by complex **1** on excitation. Similar results were obtained for complex **1a** (Fig. S13–S15, ESI†), with an additional observation of vacuolation in cytoplasm, a marker of paraptosis.[27]

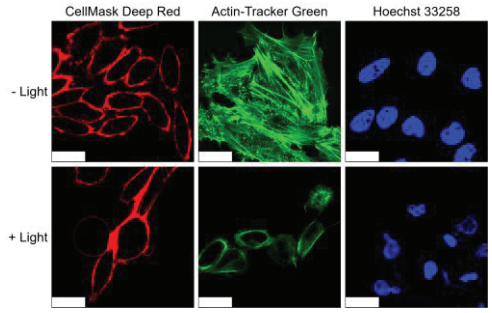

Fig. 2 Changes of plasma membrane appearance, cytoskeleton structure, and nuclear morphology in HepG2 cells pretreated with complex **1** (10 μM, 12 h) without (upper) or with (lower) irradiation at 450 nm for 5 min (10 mW cm^{-2}), then stained with CellMask Deep Red (5 μM, 15 min, λ_{ex} = 635 nm, λ_{em} = 650 − 700 nm), Actin-Tracker Green (2 μM, 15 min, λ_{ex} = 488 nm, λ_{em} = 500 − 550 nm), or Hoechst 33258 (5 μM, 15 min, λ_{ex} = 405 nm, λ_{em} = 415 − 495 nm). The cells were fixed with 4% paraformaldehyde in PBS (pH 7.2) for 15 min before actin and nucleus staining. Scale bar: 25 μm.

In summary, we have studied the impacts of the POSS moiety on the different properties of luminescent iridium(III) complexes. Although the cyclometallating ligands are the same, the photoinduced ROS generation behaviour and organelle localisation of the complexes are very different. The cellular uptake, intracellular localisation, bioimaging, and (photo)cytotoxicity studies demonstrated their applications as organelle-targeting imaging reagents and phototherapeutics.

We thank the financial support from Hong Kong Research Grants Council (Project No. CityU 11300318, CityU 11300017, CityU 11300019, CityU 11302820, T42-103/16-N, C6009-17G and C6014-20W), and "Laboratory for Synthetic Chemistry and Chemical Biology" under the Health@InnoHK Program launched by Innovation and Technology Commission (HKSAR, China). JHZ acknowledges the receipt of a Postgraduate Studentship administered by City University of Hong Kong.

Conflicts of interest

There are no conflicts to declare.

References

1 (*a*) S. Monro, K. L. Colon, H. Yin, J. Roque, P. Konda, S. Gujar, R. P. Thummel, L. Lilge, C. G. Cameron and S. A. McFarland, *Chem. Rev.*, 2019, **119**, 797; (*b*) L. K. McKenzie, H. E. Bryant and J. A. Weinstein, *Coord. Chem. Rev.*, 2019, **379**, 2; (*c*) C. Caporale and M. Massi, *Coord. Chem. Rev.*, 2018, **363**, 71.
2 L. Holden, C. S. Burke, D. Cullinane and T. E. Keyes, *RSC Chem. Biol.*, 2021, **2**, 1021.
3 R. Bevernaegie, B. Doix, E. Bastien, A. Diman, A. Decottignies, O. Feron and B. Elias, *J. Am. Chem. Soc*., 2019, **141**, 18486.
4 J. A. Roque III, P. C. Barrett, H. D. Cole, L. M. Lifshits, E. Bradner, G. Shi, D. von Dohlen, S. Kim, N. Russo, G. Deep, C. G. Cameron, M. E. Alberto and S. A. McFarland, *Inorg. Chem.*, 2020, **59**, 16341.
5 X. Liu, G. Li, M. Xie, S. Guo, W. Zhao, F. Li, S. Liu and Q. Zhao, *Dalton Trans.*, 2020, **49**, 11192.
6 W.-L. Liu, T. Liu, M.-Z. Zou, W.-Y. Yu, C.-X. Li, Z.-Y. He, M.-K. Zhang, M.-D. Liu, Z.-H. Li, J. Feng and X.-Z. Zhang, *Adv. Mater.*, 2018, **30**, 1802006.
7 X. Cui, G. Lu, S. Dong, S. Li, Y. Xiao, J. Zhang, Y. Liu, X. Meng, F. Li and C. S. Lee, *Mater. Horiz.*, 2021, **8**, 571.
8 M. Li, J. Xia, R. Tian, J. Wang, J. Wang, J. Fan, J. Du, S. Long, X. Song, J. W. Foley and X. Peng, *J. Am. Chem. Soc.*, 2018, 140, 14851.
9 K. Li, Y. Liu, K.-Y. Pu, S.-S. Feng, R. Zhan and B. Liu, *Adv. Funct. Mater.*, 2011, **21**, 287.
10 J. Jin, Y. Zhu, Z. Zhang and W. Zhang, *Angew. Chem. Int. Ed.*, 2018, **57**, 16354.
11 (*a*) A. M.-H. Yip and K. K.-W. Lo, *Coord. Chem. Rev.,* 2018, **361**, 138; (*b*) K. K.-S. Tso, K.-K. Leung, H.-W. Liu and K. K.-W. Lo, *Chem. Commun.*, 2016, **52**, 4557; (*c*) S. P.-Y. Li, C. T.-S. Lau, M.-W. Louie, Y.-W. Lam, S.-H. Cheng and K. K.-W. Lo, *Biomaterials*, 2013, **34**, 7519; (*d*) S. P.-Y. Li, H.-W. Liu, K. Y. Zhang and K. K.-W. Lo, *Chem. Eur. J.*, 2010, **16**, 8329.
12 (*a*) J.-H. Zhu, B. Z. Tang and K. K.-W. Lo, *Chem. Eur. J.*, 2019, **25**, 10633; (*b*) J.-H. Zhu, S.-M. Yiu, B. Z. Tang and K. K.-W. Lo, *Inorg. Chem.*, 2021, **60**, 11672.
13 L.-Q. Wei and B.-H. Ye. *ACS Appl. Mater. Interfaces*, 2019, **11**, 41448.
14 (a) K. Suzuki, A. Kobayashi, S. Kaneko, K. Takehira, T. Yoshihara, H. Ishida, Y. Shiina, S. Oishi and S.Tobita, *Phys. Chem. Chem. Phys.*, 2009, **11**, 9850; (b) A. A. Abdel-Shafi, P. D. Beer, R. J. Mortimer and F. Wilkinson, *J. Physic. Chem. A*, 2000, **104**, 192.
15 S. P.-Y. Li, A. M.-H. Yip, H.-W. Liu and K. K.-W. Lo. *Biomaterials*, 2016, **103**, 305.
16 L. C.-C. Lee, A. W.-Y. Tsang, H.-W. Liu, K. K.-W. Lo, *Inorg. Chem.*, 2020, **59**, 14796.
17 P. K.-K. Leung, L. C.-C. Lee, H. H.-Y. Yeung, K.-W. Io and K. K.-W. Lo, *Chem. Commun.*, 2021, **57**, 4914.
18 (*a*) P. K.-K. Leung and K. K.-W. Lo, *Chem. Commun.*, 2020, **56**, 6074; (*b*) D. Ashen-Garry and M. Selke, *Photochem., Photobiol*., 2014, **90**, 257.
19 M. S. de Almeida, E. Susnik, B. Drasler, P. Taladriz-Blanco, A. Petri-Fink and B. Rothen-Rutishauser, *Chem. Soc. Rev.*, 2021, **50**, 5397.
20 S. K. Rodal, G. Skretting, Ø. Garred, F. Vilhardt, B. van Deurs and K. Sandvig, *Mol. Biol. Cell*, 1999, **10**, 961.
21 Y. Ju, H. Guo, M. Edman and S. F. Hamm-Alvarez, *Adv. Drug Delivery Rev*., 2020, **157**, 118.
22 J. P. Piret, D. Mottet, M. Raes and C. Michiels, *Ann. N. Y. Acad. Sci.*, 2002, **973**, 443.
23 V. Novohradsky, A. Rovira, C. Hally, A. Galindo, G. Vigueras, A. Gandioso, M. Svitelova, R. Bresolí-Obach, H. Kostrhunova, L. Markova, J. Kasparkova, S. Nonell, J. Ruiz, V. Brabec and V. Marchán, *Angew. Chem. Int. Ed.*, 2019, **58**, 6311.
24 B. Jana, A. P. Thomas, S. Kim, I. S. Lee, H. Choi, S. Jin, S. A. Park, S. K. Min, C. Kim and J. H. Ryu, *Chem. Eur. J.*, 2020, **26**, 10695.
25 L. Duprez, E. Wirawan, T. Ven Berghe and P. Venabeele, *Microbes Infect.*, 2009, **11**, 1050.
26 A. Weber, J. Iturri, R. Benitez, S. Zemljic-Jokhadar and J. L. Toca-Herrera, *Sci. Rep.*, 2019, **9**, 14903.
27 X.-W. Wu, Y. Zheng, F.-X. Wang, J.-J. Cao, H. Zhang, D.-Y. Zhang, C.-P. Tan, L.-N. Ji and Z.-W. Mao, *Chem. Eur. J.*, 2019, **25**, 7012.

